ANNUAL REVIEWS

*Annual Review of Analytical Chemistry*

# Three-Dimensional Single Particle Tracking and Its Applications in Confined Environments

Yaning Zhong[1] and Gufeng Wang[1,2]

[1]Department of Chemistry, North Carolina State University, Raleigh, North Carolina 27695, USA; email: gufengwang2011@gmail.com

[2]Department of Chemistry, Georgia State University, Atlanta, Georgia 30303, USA

Annu. Rev. Anal. Chem. 2020. 13:381–403

First published as a Review in Advance on February 25, 2020

The *Annual Review of Analytical Chemistry* is online at anchem.annualreviews.org

https://doi.org/10.1146/annurev-anchem-091819-100409





## Keywords

three-dimensional single particle tracking, point spread function, PSF, astigmatic imaging, double-helix PSF, deep neural networks, confined environment

## Abstract

Single particle tracking (SPT) has proven to be a powerful technique in studying molecular dynamics in complicated systems. We review its recent development, including three-dimensional (3D) SPT and its applications in probing nanostructures and molecule-surface interactions that are important to analytical chemical processes. Several frequently used 3D SPT techniques are introduced. Especially of interest are those based on point spread function engineering, which are simple in instrumentation and can be easily adapted and used in analytical labs. Corresponding data analysis methods are briefly discussed. We present several important case studies, with a focus on probing mass transport and molecule-surface interactions in confined environments. The presented studies demonstrate the great potential of 3D SPT for understanding fundamental phenomena in confined space, which will enable us to predict basic principles involved in chemical recognition, separation, and analysis, and to optimize mass transport and responses by structural design and optimization.

## 1. INTRODUCTION

Single particle tracking (SPT) is a set of methods to observe and analyze the position and motion of individual particles or molecules. The object of SPT can be individual particles or molecules, which will be generally called particles in this review. SPT includes single particle localization, from which the particle position as a function of time is acquired and the trajectory constructed. The trajectory of a single particle contains important information about the structural and physicochemical properties of the medium it is in, as well as the interactions between the particle and its environment.

In the biological sciences, SPT has been proven to be a powerful technique in studying biological processes (1–12). Prominent examples include resolving of individual steps for molecular motors such as myosin and kinesin (13, 14). In addition, single-molecule localization has been a major milestone for superresolution optical imaging, which discloses unprecedented structural details of biological systems (7, 8). Currently, SPT has been used to probe a variety of cellular activities. Its biological applications have been reviewed elsewhere (2, 3, 15, 16) and are beyond the scope of this article.

Although a major push for the development of SPT techniques comes from the biological research communities, SPT is also extensively used in non-life sciences. Especially of interest to analytical chemists is its capability to probe interactions between molecules and surfaces, whether that is a flat model surface or curved surface in a porous material. Such interactions, and the resulting molecular binding and mass transport, play an important role in analytical chemistry, such as separation, electrochemistry, sensors, and other surface techniques. For example, dating back to the 1990s, Prieve, Bevan, and colleagues used total internal reflection fluorescence (TIRF) microscopy to study the van der Waals interaction between colloidal particles and a wall (17–19). Schwartz and coworkers (20–22) systematically studied molecules' mass transport at the liquid–solid interface, and a model was proposed to explain the observed non-Brownian surface diffusion. Higgins et al. (23, 24) studied the confinement effect on molecular mass transport in one-dimensional nanopores. Yeung's group (25, 26) investigated DNA/protein molecules and nanoparticles' migration near a flat surface and in cylindrical micropores. They found that attractive interaction in chromatography processes can extend to an extraordinarily long distance from the wall. Similarly, particle or molecule binding and transport have been studied in three-dimensional (3D) microporous polymers (27), in protein ion-exchange chromatography stationary phase (28), and in reverse-phase high-performance liquid chromatography (HPLC) stationary phase (29). Fang and coworkers (30) monitored catalytic reactions and subsequent molecular transport on porous silica coated metal catalysts. They surprisingly found that the porous silica coating increases rather than slows down the heterogenous reaction rate, which indicates that confinement of the reactant molecules can play a role in promoting the reaction speed (30). These studies helped our understanding of fundamental processes at interfaces, which are crucial to analytical techniques.

Currently, most of the SPT techniques can only track 2D motion of the particles. However, sample media in real world are 3D in nature and the particle probes usually move in a tortuous and congested 3D space that is highly scattering. Developing robust 3D SPT techniques is thus crucial for disclosing the complete structural information and dynamic interactions in the full 3D space. Recently, great efforts have been made to develop 3D SPT techniques for this purpose. So far, a very limited number of studies have been reported that are relevant to analytical science. This review focuses on 3D SPT techniques that are especially of interest to analytical chemists; corresponding data analysis methods and selected case studies are also reviewed.

## 2. EXPERIMENTAL METHODS

### 2.1. Z-Information in Optical Imaging

It is important to point out that conventional diffraction-limited (or Airy disc-patterned) optical microscopy actually gives partial z-information in a 2D image. When a particle is moved out of the focal plane, the diffraction ring pattern becomes more apparent given that the image signal-to-noise ratio (S/N) is sufficiently high (**Figure 1*a***). Many studies have shown that the radii of the rings change as a function of the particle distance away from the focal plane (31). However, it is usually inconvenient to obtain the particle's full 3D position using these diffraction rings for two main reasons: (*a*) The symmetry with respect to the focal plane causes sign ambiguity of the particle position along the z-axis, and (*b*) this method works best for the particle in a defocused position at which the diffraction ring pattern is clear. The image pattern is insensitive to the particle's z-position near the focal plane, at which the particle gives the strongest signal.

In order to obtain the 3D position of a particle conveniently, many methods have been employed in real applications. Depending on their working principles, current 3D localization techniques can be classified into three main categories: multiplane scanning (either at the sample side or the image side), tuning the spatial excitation/emission profile (at the sample side), and point spread function (PSF) engineering (at the image side).

### 2.2. Multiplane Scanning

The 3D position of a particle can be obtained by scanning the sample with respect to the objective along the z-axis for multiple images (i.e., sample side scanning). The z-stack images can be acquired using either wide-field imaging (e.g., bright-field, dark-field, differential interference contrast microscopy, etc.) (32) or point detection–based confocal imaging. It is quite time consuming to collect a whole stack of images to determine a particle's z-position. However, the temporal resolution of this approach can be significantly improved by reducing the total number of the z-images (31, 33–37) or the total signal collection spots in confocal imaging (38–40).

**2.2.1. Confocal imaging-based 3D single particle tracking.** In the confocal imaging approach, it is realized that the particle's 3D position can be determined by collecting the emission from a minimum of four tetrahedrally distributed detection spots in the image space (**Figure 1*b***) or by collecting the emission from four excitation spots in the sample space. Tracking is then achieved by a simple feedback loop in which the laser spot is moved to be near the current probe position and scans the sample space at four spots for the next probe position. This process is repeated until a sufficiently long trajectory is acquired or the signal disappears. Several groups have developed confocal fluorescence microscopy-based 3D tracking by using this approach (39, 41–43). The temporal resolution can be as low as below 1 ms/frame (38, 39, 41, 44, 45).

Compared to current wide-field imaging-based 3D tracking techniques, which usually have a z-working distance of several micrometers due to limited depth of field, confocal imaging-based 3D tracking can have a much wider z-range of tens to hundreds of micrometers without any additional equipment. The shortcomings are expensive instrumentation, tracking limited to one particle at a time, the high tendency of losing the particle, and relatively low precision (50–100 nm).

**2.2.2. Bifocal plane imaging.** Instead of scanning the particle at the sample side, z-information can also be obtained by scanning the detector (camera) at the image side of the microscope. However, owing to the design of modern microscopes, scanning the detector is usually inconvenient.

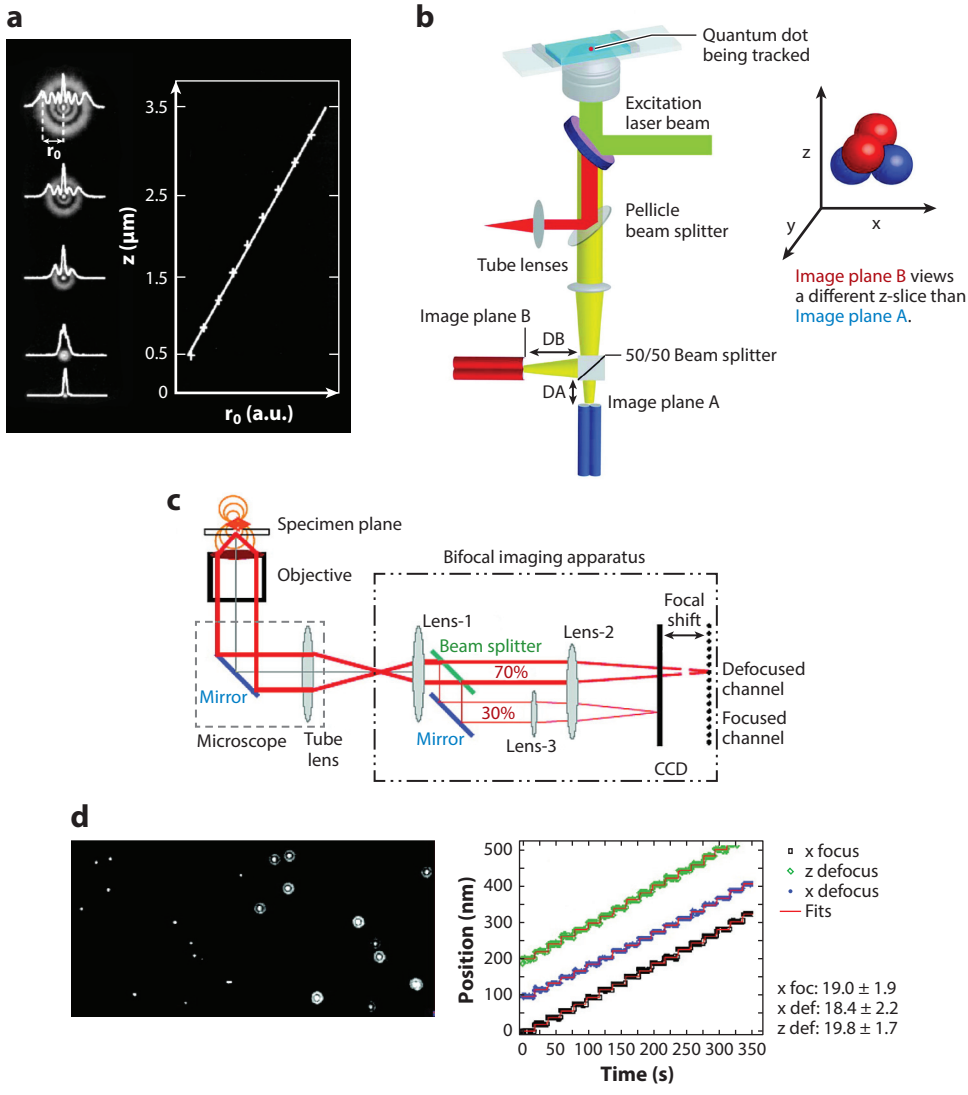


**Figure 1**

Z-information in an image and multiplane scanning-based 3D single particle tracking. (*a*) The linear relation between the radii of the diffraction rings and defocused z-distance in diffraction-limited microscopy. Adapted with permission from Reference 31. Copyright 2003, Optical Society of America. (*b*) Confocal imaging setup and the tetrahedrally distributed detection spots for localizing a particle in the 3D space. Adapted with permission from Reference 38. Copyright 2010, American Chemical Society. (*c*) Schematic of bifocal plane imaging. (*d*) Representative paired images acquired in bifocal plane imaging and recovered z-position in z-stepping experiments. Adapted with permission from Reference 33. Copyright 2007, American Chemical Society.

In wide-field imaging-based 3D tracking, this approach can be used by the application of beam splitters and mirrors since the total number of z-slices is limited. Because the minimum number of the z-frames is two to unambiguously determine a particle's z-position, simultaneous collecting images at two z-planes at the image side is required. This can be achieved by splitting the image

light beam into two: one imaged at the focal plane and the other at a slightly defocused plane (**Figure 1*c***) (33). The two image light beams can be projected to the same camera chip so only one camera exposure is needed (**Figure 1*d***). The particle's z-position can then be recovered by comparing the two images' patterns or intensities.

A variation of this method is achromatic aberration-based bifocal plane imaging (46). In this approach, the image light beam is split into two color channels by a dichroic mirror. The two light beams have different focal planes due to achromatic aberration of the microscope objective. When projected to the same camera chip, one light beam can be focused and the other slightly defocused, giving sufficient information to recover the particle's z-position.

The main advantages of bifocal or even multiple focal plane imaging are high position accuracy and precision (~10 nm), fast imaging rate (video rate), and the ability to acquire long trajectories. The disadvantage is that the instrument needs a major customization to allow the image light beam splitting and realignment so that the two beams can be projected to the same camera chip. Alternatively, a major add-on accessory named the DualView multichannel imaging system may achieve similar functions but needs additional customization.

## 2.3. Tuning the Spatial Excitation/Emission Profile at the Sample Side

Axial tracking can also be achieved by using a second group of techniques: tuning the excitation or emission profile at the sample side. The z-position of a particle can then be recovered from the particle intensity or other properties that are determined by the excitation/emission profile.

**2.3.1. Total internal reflection fluorescence microscopy.** The most frequently used method in this group is total internal reflection fluorescence microscopy (TIRFM) (47, 48), which uses an interface to define the excitation intensity along the z-axis. Unlike other wide-field florescence microscopy, the excitation in TIRFM is by the evanescent field at a total internal reflection surface. The evanescent field intensity $I$ decays exponentially as a function of the distance $z$ from the TIR surface (48):

$$I(z) = I(0)\exp\left(-\frac{z}{d}\right), \qquad 1.$$

where $d$ is the penetration depth of the evanescent field determined by the wavelength of the light, the refractive indices of the materials at either side of the TIR interface, and the light incident angle. Consequently, the fluorescence emission intensity, which is proportional to the excitation intensity, can be used to recover particle's z-position.

TIRFM has been used to study particle–surface interactions since the early 1980s (17). More recent publications by Fang's group (6, 49) first reported the 3D active site distribution on a frequently used catalytic platform, which consists of a solid silica core, a mesoporous silica shell, and uniformly distributed Pt nanoparticles sandwiched in between. The 3D active site map was constructed by imaging single fluorescent molecules produced at active sites followed by 3D localization: the lateral position that was obtained from the centroid of the single-molecule image spot and the z-position from the intensity. A globular distribution of the active sites was recovered, representing the Pt nanoparticles deposited on the silica spherical core. This approach shows the great potential of TIRFM, which enables one to establish the structure-catalytic activity relationship in real 3D heterogeneous catalysts that are highly porous and scattering.

**2.3.2. Fluorescence lifetime imaging microscopy and fluorescence-interference contrast microscopy.** The second group of methods can also tune the spatial emission profile by introducing factors that affect the emission. For example, fluorescence lifetime imaging microscopy

(FLIM) (50) utilizes the lifetime of fluorescent molecules near a metal or silicone surface to determine its z-position: The molecules are quenched to different extents so they have different fluorescence lifetimes, from which their z-positions can be estimated. Because quenching from a surface is a relatively near-field effect, the working distance of this approach is short, ~100 nm.

Another example is fluorescence-interference contrast microscopy (FLIC) (51), which is based on interference between the direct fluorescence emission and the reflected emission from a nearby surface. The optical path lengths for the direct emission and reflected emission are different for the particle at different z's, leading to constructive or destructive interference and thus enhanced or reduced intensity on the detector. The z-position of the fluorophore can then be recovered from the collected fluorescence intensity. Using this method, the corkscrew-like motion of quantum dots attached to a microtubule (diameter ~25 nm) gliding and rotating on a silicon surface was observed.

To summarize, the second group of methods imposes a position-excitation/emission relationship at the sample side of the microscope so that their z-position can be determined. They provide new perspectives on the design of 3D SPT techniques. In particular, TIRFM has a very shallow excitation depth and consequently very low image background, which makes it an ideal tool to study low signals from single molecules. It has been used as an independent imaging platform or in combination with other imaging techniques to achieve new functionalities (52).

The shortcoming of this group of methods for 3D SPT is apparent. (*a*) They usually need to engineer the sample or the sample substrate, e.g., the addition of an interface near the sample, which limits the generality of their application. (*b*) The z-working distance is usually short (~100 nm) when a near-field effect of the interface is employed.

## 2.4. Point Spread Function Engineering at the Image Side

The axial information can be obtained through a third group of methods: those that tune the PSF and make it z-sensitive, where PSF is defined as the spatial light intensity distribution in the 3D space at the image side for a point-emitting object. As mentioned earlier, in conventional diffraction-limited microscopy, a single z-slice of the 3D PSF contains partial z-information that is inconvenient to recover. To unambiguously and accurately recover the z-position, information from multiple z-slices is required. Thus, it can be understood that to minimize the camera exposure number to 1, as much useful information as possible in the 3D PSF should be collected in a single image. Or, in other words, both in-focal and out-of-focal plane signals that would have been in a conventional microscope need to be selected through engineering to show up in one image to facilitate the z-localization. This process requires changing the PSF of a microscope, usually at the image side. Thus, it is named PSF engineering. Frequently used approaches including astigmatic imaging (52, 53), double-helix PSF imaging (54, 55), and parallax imaging (56) are discussed below.

**2.4.1. Astigmatic imaging.** A straightforward method to realize PSF engineering is to create astigmatism in the imaging system. This can be achieved by inserting a weak cylindrical lens into the imaging optical path, either after the microscope objective or after the tube lens (**Figure 2*a***), to create two slightly shifted focal planes: one for horizontal rays and one for vertical rays (**Figure 2*b***). Depending on the strength of astigmatism, the image pattern of a point object can vary from an ellipse (52) (aspect ratio changing with respect to emitter's z-position) to an expanded diamond-like shape (**Figure 2*c,d***) (53), which allows the z-coordinate of the emitter to be unambiguously determined from one image.

Astigmatic imaging was first introduced by Kao & Verkman (57). It became popular in recent years ever since it was applied to stochastic optical reconstruction microscopy (STORM) to

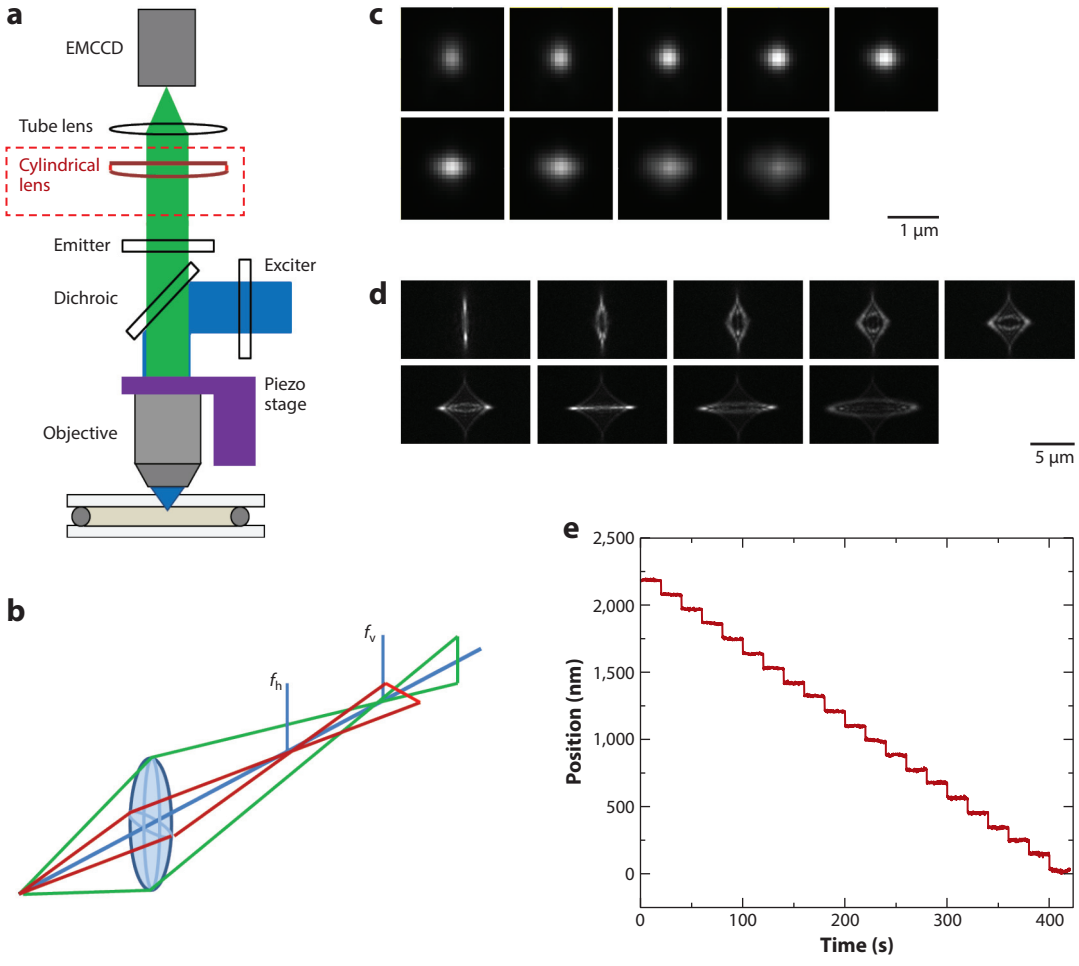


**Figure 2**

Astigmatic imaging-based 3D single particle tracking. (*a*) Schematic of the instrument setup. (*b*) Focusing of horizontal and vertical rays. (*c*) Representative image slices of the elliptical PSF. The focal plane gap was ~1 μm. The z-step size between images was 200 nm. (*d*) Representative image slices of the expanded, diamond-like PSF. The focal plane gap was ~5 μm. The z-step size between images was 1.00 μm. (*e*) Recovered z-position in a stepping experiment using the expanded astigmatic PSF. Panels *a*, *d*, and *e* adapted with permission from Reference 53. Copyright 2016, the American Chemical Society. Abbreviations: EMCCD, electron multiplying charge-coupled device; PSF, point spread function.

achieve 3D superresolution, which has a lateral resolution of ~20 nm and an axial resolution of 50 nm (52). Because this method is simple in both instrumentation and data analysis, it is popularly used in 3D SPT.

Note that the astigmatic PSFs can vary from small ellipses to large diamond-like shapes, depending on the strength of astigmatism. The rationale for using expanded PSFs is that the more dispersed the PSF, the more sensitive its image pattern to the particle's z-position. The working distance also becomes larger. When the photon flux is sufficient, the expanded PSF is advantageous in localization accuracy and precision. However, in practice, larger image dispersion means lower photon counts per camera pixel, which impairs localization. It is a compromise in selecting

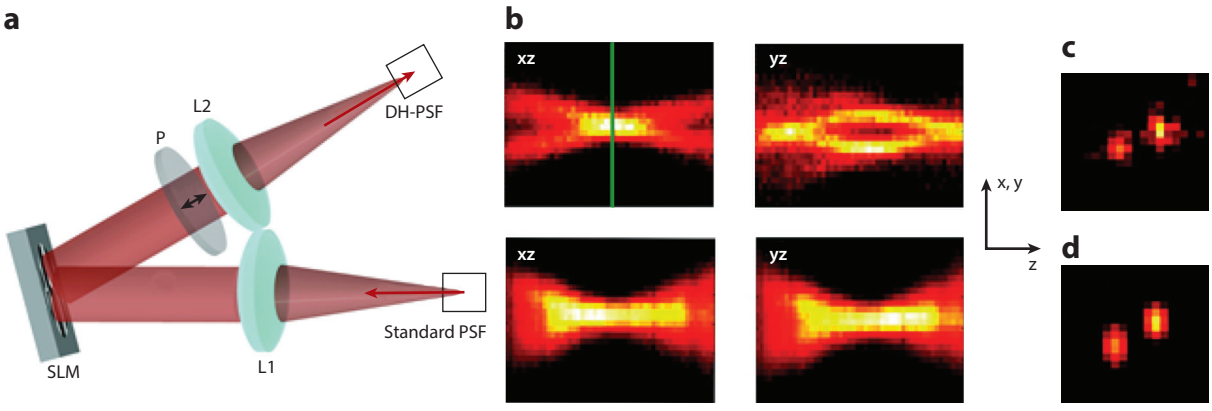


**Figure 3**

Double-helix point spread function (DH-PSF) for 3D single particle tracking. (*a*) Schematic setup. (*b*) Top panels are xz and yz cross sections of a DH-PSF whereas the bottom panels are from the standard PSF from a conventional microscope. (*c*,*d*) Real-space image pattern and its fitting output. Adapted with permission from Reference 55. Copyright 2009, American Chemical Society. Abbreviations: L, lens; P, image plane; SLM, spatial light modulator.

the proper PSFs for specific studies. Zhao et al. (53) used expanded astigmatic PSF to study fluorescent particle diffusion in cylindrical nanopores. The gap between the horizontal and vertical ray focal planes was tuned to ~5 μm (53, 58) in contrast to ~1 μm for elliptical PSFs. As such, it can observe up to 10 μm into the substrate with an axial localization precision of ~20 nm for 100-nm fluorescent polystyrene particles (**Figure 2*e***). The time resolution can be up to 8 ms/frame (59).

**2.4.2. Phase plate-based point spread function engineering.** The diffraction-limited PSF (i.e., Airy discs) can also be modified by changing the amplitude and/or the phase profile of the image light beam behind the microscope objective. A popular method today is the double-helix PSF, which is generated by inserting a double-helix PSF phase mask (54, 55, 60) in the detection optical path in a conventional fluorescence microscope. A pair of image spots (or two lobes at high S/N) form and continuously rotate around a common center as the point emitter's z-position changes (**Figure 3**). The 3D PSF has a double-helix shape and is thus named the double-helix PSF. Moerner and coworkers (54) demonstrated that this method shows ~10 nm localization capability along the x, y, and z dimensions even with weak emitters.

It is worth noting that double-helix PSFs are possibly one of the two most used 3D localization methods, together with astigmatic PSFs. The advantages of double-helix PSFs include easy instrumentation and data analysis. Compared to astigmatic PSFs, the size of the pair of image spots in a double-helix PSF is mostly the same throughout the depth of field, meaning that the z-localization is robust against noises in a wide z-range.

Phase masks are easy to implement. With the help from spatial light modulators, designing new phase plates became simpler. A variety of phase mask–based PSF engineering methods emerged and showed excellent 3D localization performance. These include tetra pods (61), corkscrew (62), self-bending (63), extended double-helix PSFs (64), and others.

**2.4.3. Translated point spread functions or parallax imaging.** The third type of PSF engineering method encodes axial position information using translated PSFs, or parallax imaging (56). This method was first introduced by Yajima and coworkers (56), who employed a wedge

prism at the back focal plane to divert the direction of half of the image light beam. As a result, a pair of split image spots along the *y*-axis will form at the image plane for a point-emitting object. The displacement of the point object in the *z*-axis shifts the relative position of the split images along the x-direction, from which the defocused distance of the point object can be recovered. The corkscrew-like motion of particles attached on gliding and rotating microtubules was for the first time directly observed using this technique. Because this approach is similar to viewing the same object from two different positions, like how human beings view a distant object, it is named parallax imaging. Similarly, parallax imaging can be achieved using a pair of closely spaced mirrors, or a bisected, linearly ramped spatial light modulator to split the image light beam (65, 66).

To summarize Section 2.4, all of these PSF engineering methods can be applied on current commercial microscopes with simple modifications to achieve 3D SPT. Thus, they are of interest to a wide range of labs, including analytical chemistry labs.

### 2.5. 3D Single Particle Tracking for Nonfluorescent Particles

Thus far, all of the techniques we have reviewed were developed for fluorescence microscopy. For nonfluorescent probes, other modes of microscopy need to be used, such as dark-field microscopy. The aforementioned 3D localization principles can be adapted for these nonfluorescent detection techniques with little modification.

It is worthwhile to note the special type of detection scheme for nonfluorescent particles: the interference-based detection that is used to enhance imaging sensitivity. The scattering from small particles scales with their radius to the sixth power so the signal drops quickly as the particle size becomes smaller. In interference-based imaging, a reference beam is introduced to interfere with the scattering signal, which brings the signal level up to their radius to the third power (67). Thus, the signal is enhanced. One such detection technique is interferometric scattering (i-SCAT) microscopy, which can detect gold nanoparticles as small as 5 nm (68). Interestingly, the 3D interferometric PSF has a unique, asymmetrical ring pattern along the *z*-axis, allowing their xyz positions to be determined from a single exposure (69). This detection scheme is powerful, yet a laser beam is required, which adds to the cost and complexity of the instrument.

## 3. DATA ANALYSIS

Among all of the 3D SPT techniques reviewed above, the PSF engineering methods introduce 3D resolution in one image. They require a simple instrument but no special sample geometry. However, these methods may involve more complicated image patterns, which makes data analysis challenging. To recover the 3D position of a particle from an image, a reliable estimator is required. It needs to be established through the standard calibration procedures, which involves the collection of calibration images at different z-positions, image pattern analysis, the establishment of an image feature-z relationship, and the same image pattern analysis for the samples (70, 71). The key procedure is the image pattern analysis.

Generally, analysis of image data can go through two routes:

1. When the image pattern is relatively simple, image features can be extracted and a feature-z relationship can be established using the calibration set; the z-position of a sample image is determined depending on its feature. The image feature vector can be as simple as only one variable, such as the aspect ratio of the astigmatic image spot or the rotating angle of the paired image spots in double-helix PSF. To extract clearly defined image features, one needs to be able to predict the image patterns and approximate the experimental images

to the theoretical ones. Nonlinear least squares fitting is the most frequently used method (52). More sophisticated statistical methods such as maximum likelihood estimation (72) were also introduced to improve the extraction accuracy. Data analysis methods using this approach have been studied and their accuracy and precision as a function of the photon flux have been presented in recent studies (73–76). Here, we do not discuss these methods but focus on more complicated PSFs and their analysis methods below.

2. When the image pattern is so irregular that the PSF cannot be described using a simple function, the calibration and data analysis cannot use the aforementioned approach and become more challenging. In fact, complicated PSFs are frequently encountered and are of more general importance in a variety of imaging techniques (e.g., DIC imaging, defocused imaging), including 3D localization. For example, at a high S/N, the frequently used double-helix PSF shows a pattern of two asymmetrical rotating lobes (77). For astigmatism-based imaging, the PSF deforms and changes from an elongated circle to a cross and then a diamond shape when the astigmatism strength increases (53). Similar irregular patterns can be found in other methods such as wedge prism and tetrapod PSFs. Even worse, due to optical aberrations of individual imaging systems and different experimental conditions, it is challenging to predict the exact PSF patterns. In this case, a general data analysis approach without clearly defining the image features is needed to analyze these images.

### 3.1. Complicated Image Pattern Recognition for 3D Localization

Data analysis for irregular image pattern–based single particle 3D localization, by essence, is an image classification process, which classifies sample images into categories (i.e., z-positions) defined by calibration image sets. There are multiple methods for image classification, from the simple correlation coefficient method to supervised machine learning algorithms and deep neural networks.

The Pearson correlation coefficient method is a universally applicable and arguably the most reliable pattern recognition method (78). In this method, the sample image is compared pixel by pixel with each image in the calibration set. The similarity is determined based on the correlation coefficient $p$, which is defined as

$$p(\text{sample, model}) = \frac{1}{m-1}\sum_{i=1}^{m}\frac{[I_{\text{model}}(i) - I_{\text{model}}(avg)]}{\sigma_{\text{model}}}\frac{[I_{\text{sample}}(i) - I_{\text{sample}}(avg)]}{\sigma_{\text{sample}}}, \qquad 2.$$

where the summation is over all of the $m$ pixels in the sample image, $I$ is the intensity, and $avg$ and $\sigma$ denote the average and standard deviation of all intensities in the model (i.e., the image in the calibration set) or the sample, respectively. For sparse calibration sets (i.e., the number of calibrated z-values is sparsely distributed over the whole z-range), a weighing or fitting procedure is usually used to obtain subframe resolution (53).

The correlation coefficient method is a simplified linear machine learning method, which presumes that the calibration image sets are a well-trained model and uses this model to evaluate the experimental data. This is true only when experimental data and calibration data are collected under the same experimental condition and have high image quality, including high S/N and low interfering background. With these restrictions, the correlation coefficient method does show decent localization accuracy and precision (53). However, in realistic conditions, when noise and background interference cannot be avoided, the method shows its limitations because the assumption is no longer valid.

More sophisticated machine learning methods (79) train models with a decision function $Y = f(\mathrm{X})$, or equivalently, the conditional probability distribution $P(Y|X)$, in which $X$ stands for input

data, and *Y* stands for classification result. Depending on how the decision function is obtained, there are two main groups of supervised learning approaches: generative approaches [e.g., Naïve Bayes (79)] and discriminative approaches [e.g., logistic regression/maximum entropy model (80)]. The generative approaches generate the decision function (or the joint probability distribution) directly from the constraints (i.e., data in the training set), while the discriminative algorithm only explores and optimizes the decision function in a given hypothesis space for models.

Traditional machine learning algorithms have been applied in SPT and some achievements have been made (73). However, they are not generally used partly because of their intrinsic deficiency in analyzing large and complicated images: First, the machine learning models are usually too simple to model image data that contain multiple relevant and irrelevant features; second, machine learning algorithms perform poorly for large image data due to convergence and overfitting issues.

## 3.2. Deep Neural Networks

Zhong et al. (81) show that by using deep neural networks (DNNs), recognition and differentiation of similar, complicated z-image patterns can be satisfactorily achieved. DNNs are a type of forward-feeding artificial neural network inspired by animal visual cortex organization (70, 71, 82–84). One of the biggest successes of DNNs is their image pattern recognition in complex, highly interfering backgrounds, as shown in recent high-profile image recognition contests (82, 83, 85). In fact, practical facial recognition in the presence of background had been a difficult problem for many years, but solutions have been developed recently since the introduction of DNNs.

In traditional machine learning methods, the sample images and the logical results are directly linked in the regression process. In contrast, in a DNN, there are multiple hidden layers in between, which is why it is named deep learning (**Figure 4*a***) (70, 84). In the shallow layers, the local and simple features such as lines, corners, and edges are extracted, while in the deep layers, more global and complicated profiles are extracted because these layers have a larger receptive field. In the regression process, these multiple hidden layers bearing information about special features of the image at multiple levels are fully connected, resembling how a neural network works. Thus, this method achieves high-level extraction of image features and ideally is more resistant to noises and other interferences.

Zhong et al. (81) introduced DNNs to 3D SPT techniques with the expanded astigmatic PSF. They showed that a DNN-based algorithm is more resistant to noises for image pattern recognition and particle z-localization. For high S/N images, both DNN- and correlation coefficient–based methods perform well. However, when the S/N drops to ~1, the correlation coefficient method completely fails, whereas DNNs show strong resistance to both artificial and experimental noises (**Figure 4*b***). This excellent result is achieved by optimizing the training depth: as the training depth becomes deeper in DNNs, the reported z-probability distribution for an arbitrary image becomes narrower, which indicates that more image features are extracted and considered in the calibration process (**Figure 4*c*,*d***). However, a training that is too deep may also cause overtraining, which means it falsely recognizes noises as the signal, and the recovered probability distribution becomes noisier. The localization precision becomes worse. An optimized DNN shows more resistance to noise, which potentially allows one to reduce camera integration time significantly. As a result, the frame integration time can be shortened by 1 to 2 orders of magnitude from microseconds to 50 μs compared to current methods without losing accuracy significantly. This study sheds new light on developing robust image data analysis methods and improving the time resolution for 3D SPT.

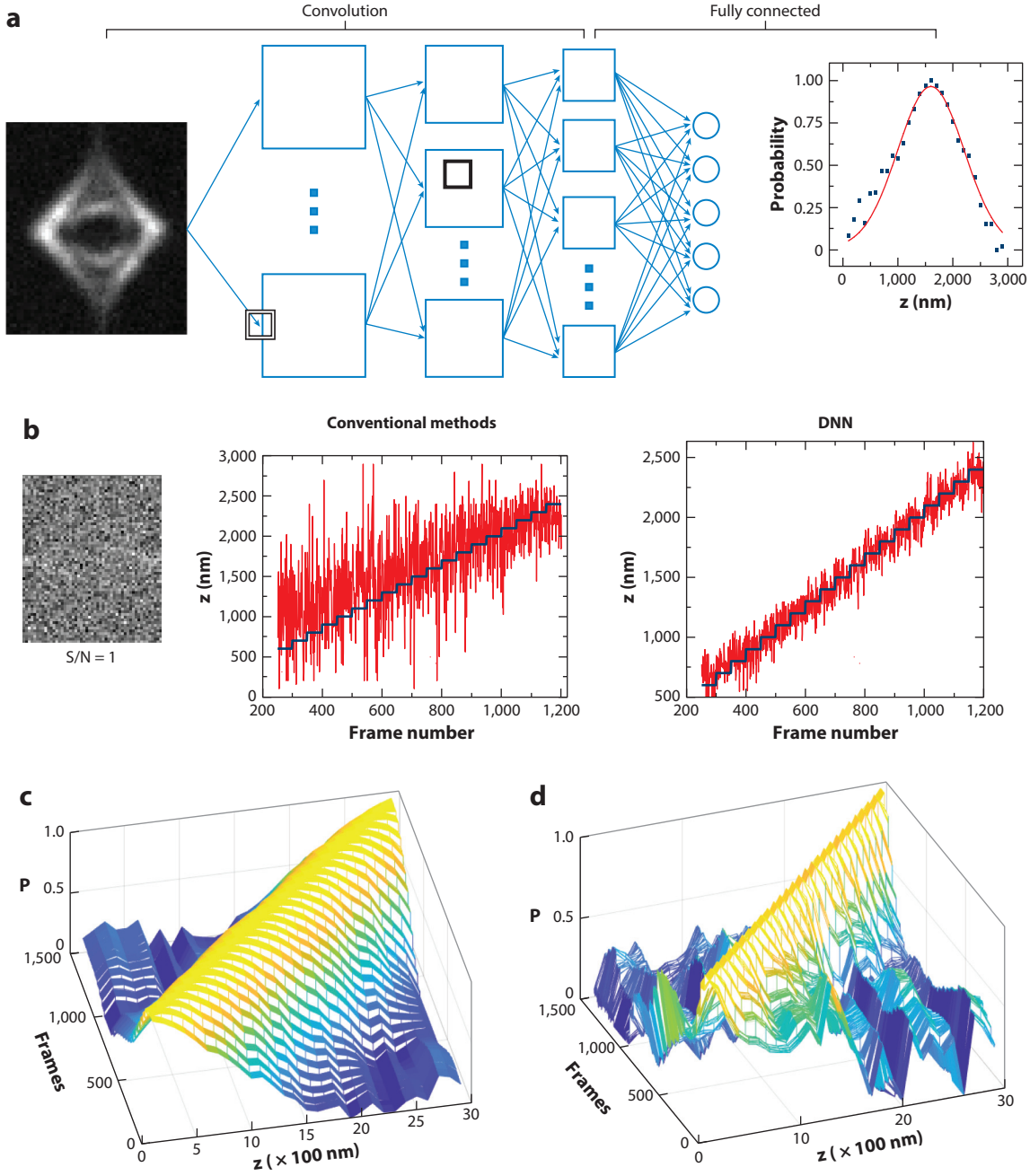


**Figure 4**

Deep neural network (DNN)-based algorithm for 3D single particle tracking using the expanded astigmatic point spread function. (*a*) Schematic of a convolutional neural network. (*b*) For an image signal-to-noise ratio (S/N) of 1, the conventional correlation coefficient method completely fails to recover the steps, whereas the DNN-based method is barely affected. (*c*) 3D presentation of the reported probabilities for images in a stepping experiment using a single-layer neural network (shallow training). A total of 19 steps were made, and each step has 50 images. (*d*) Reported probability distribution for the same stepping experiment using a 20-layer neural network (deep training). Adapted with permission from Reference 81. Copyright 2018, American Chemical Society.

## 4. APPLICATIONS OF 3D SINGLE PARTICLE TRACKING IN CONFINED ENVIRONMENTS

### 4.1. Nanoconfined Environments and Molecule-Surface Interaction

Understanding interfacial phenomena is important not only to fundamental sciences but also emerging applications such as those in human health and renewable energy (86–92). Especially of interest are media that show nanoconfinement, e.g., voids, pores, extended tubes, and planar channels, where molecules are confined by interfaces within a length scale of nanometers. These materials are broadly used in analytical techniques such as separation (28, 29, 93–95), electrochemistry, sensors, and micro- to nanofabricated tools (96). Molecular transport processes such as diffusion, migration, and adsorption/desorption in nanoconfined environments can be significantly different from those in bulk solution (25, 26, 97–104). Having a thorough understanding of mass transport and molecule-surface interaction in a confined space will enable us to predict basic principles involved in chemical recognition, separation, and analysis, and optimize mass transport and responses by material structure designing.

Thus far, our capability to investigate these problems is still limited by technical challenges. In particular, insufficient spatial resolution in the z-direction hinders our understanding of phenomena in these 3D structures. 3D SPT opens up a new avenues and allows us to probe interactions between particles and molecules with surfaces, whether on a flat model surface or the surface in porous media. Practically, 3D SPT will enable us to (*a*) probe nano- to mesostructures in situ, i.e., under working conditions; (*b*) probe particle–surface interactions in a confined space; and (*c*) monitor particle movement in the 3D space under active control. There remain a limited number of studies using 3D SPT to approach these problems; we selectively review a few important case studies.

### 4.2. Probing Local Nanostructures

The 3D trajectory of a particle in part reflects the physical confinement of the environment on the particle. Thus, it can be used to in situ probe nano- to mesostructures that are challenging to measure using other methods. For example, Zhao et al. (53) studied the particle 3D diffusion in anodic aluminum oxide membrane filters that contained cylindrical pores using the expanded astigmatic PSF. They were able to observe fluorescent polystyrene nanoparticles diffusing in and out of the anodic aluminum oxide membrane filters. **Figure 5** shows that a particle diffuses in one pore, moves out of the pore, diffuses in the bulk solution briefly, and enters another pore. The recovered 3D trajectory in part reflects the nanopore's cylindrical geometry. It was found that the pores are not perfectly cylindrical: They show slight twisting and distortion. Such tortuosity information discloses how far the actual condition can deviate from the ideal model. More interestingly, it was observed that particles can move from one pore to its neighboring pore inside the membrane filter, indicating that the pores are interconnected by defects. Such particles crossing over were commonly observed, again showing detailed structural information and an assessment of actual conditions in the model system that are challenging to measure and usually ignored.

In another study, Zhong & Wang (58) used 3D SPT to study lipid membrane morphology changes at different pHs by attaching fluorescent polystyrene nanoparticles on glass-supported lipid bilayers. They found that at neutral pHs, supported lipid bilayers show a mainly planar structure. There are also rare defects, which were captured in the 3D particle trajectory. **Figure 6** illustrates an example of a micrometer-sized bulge protruding from the plane, showing the capability of 3D SPT to probe 3D structures in a highly dynamic environment. When the solution pH

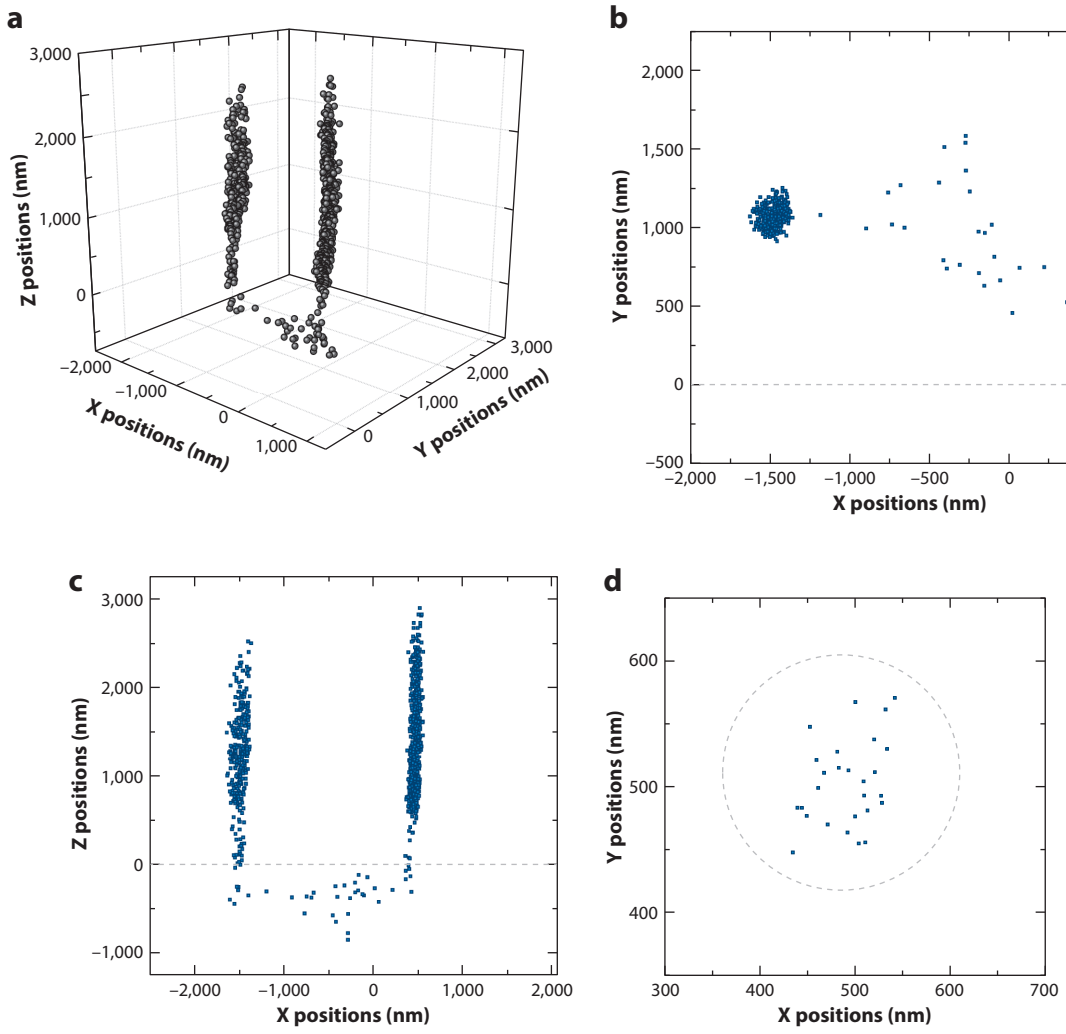


**Figure 5**

Three-dimensional particle trajectory when diffusing in and below an anodic aluminum oxide (AAO) membrane filter. (*a*) 3D view, (*b*) top view, (*c*) side view. (*d*) The top view of the particle distribution in a thin slice in the z-direction. Adapted with permission from Reference 53. Copyright 2016, American Chemical Society.

was tuned to be basic at 10.0, transiently confined diffusions of the particles with a lateral size of ~100–200 nm were frequently observed, similar to those entrapments of the probe by lipid domains reported in the literature. Most interestingly, these areas that trap the particles showed 3D bulged structures protruding from the planar lipid bilayer. These 3D structures trapped the particles for a short period of time (~0.75 s) with an estimated escape activation energy of ~4.2 $k_B T$. Nonuniform distribution of pH-sensitive lipids in the membrane was proposed to explain the formation of these 3D heterogeneous structures.

This work for the first time suggests that the geometry of the 3D lipid structures can play a role in tuning the particle–lipid surface interactions. Further research is needed to investigate whether these heterogeneous 3D structures are traditionally defined as lipid domains, which show lateral

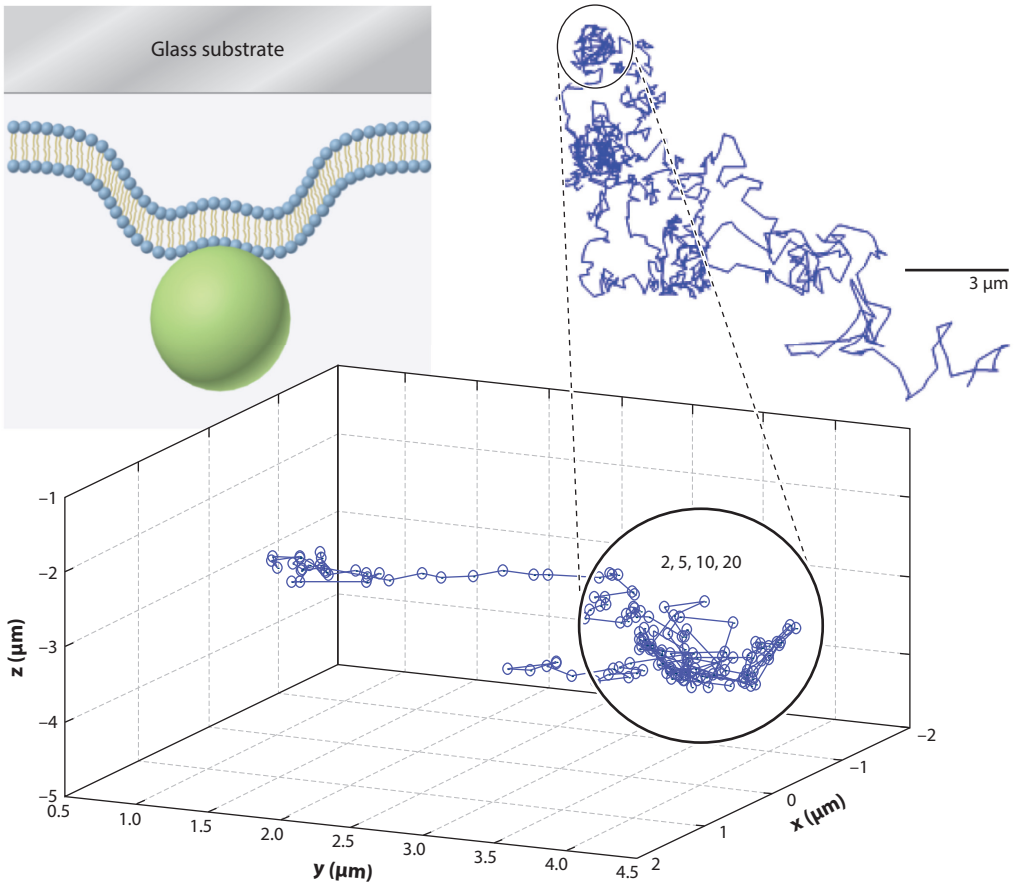


**Figure 6**

Morphology of solid supported lipid bilayer probed using 3D single particle tracking at pH 7.4. Adapted with permission from Reference 58. Copyright 2018, American Chemical Society.

phase segregation. Nevertheless, it sheds new light on the origin, structure, and function of lateral heterogeneity in a conventionally viewed 2D lipid membrane.

## 4.3. Probing Particle–Interface Interactions in Confined Environments

As stated earlier, understanding molecule-surface interactions and mass transport in porous media is important to a range of analytical techniques and beyond. Numerous studies have been carried out to investigate dynamic behavior of molecules and nanoparticles in confined environments. So far, most of these studies are limited by tracking particles in the 2D plane, whereas the complete understanding of interfacial transport relies on the 3D motion of the particles even on a flat model surface.

Molecule-surface interactions directly play a role in the molecular mass transport in a confined space. To have a better understanding of the interactions, Schwartz and coworkers (105) studied the 3D feature of molecular interface diffusion on a series of flat model surfaces. It has been hypothesized that "hops" of the molecules or particles through the solution above dominate the molecular motion on and near the surface, while the nature, origin, and details of the hops

are largely unclear. They used double-helix PSFs to track fluorescently tagged individual human serum albumin molecules with a spatial precision of 15–20 nm in 3D and a time resolution of 0.1 s. It was found that during the hops, the molecules encounter multiple unproductive contacts with the surface before being readsorbed on the surface stably. The average failed collision number increases as the surface repulsion increases. Moreover, the duration and distance of the hops are also favorably elongated by the surface repulsion while the waiting time between hops increases with respect to the attractive interaction strength. As such, the motion of the molecules on and near the surface no longer follows simple Brownian motion but is biased by short- and long-range adsorbate-surface interactions. This study provides a detailed picture of the behavior of biomolecules in the process of mass transport near a surface and is valuable to multiple industrial applications, including molecular separation.

Zhao et al. (53) studied slow mass transport in cylindrical nanopores in anodic aluminum oxide (AAO) membrane filters using 100-nm polystyrene nanoparticles (**Figure 5**). Under two model conditions, (*a*) increased solvent viscosity, which slows down the particle throughout the whole pore and solution, and (*b*) increased pore wall affinity, which only slows down the particle at the wall in theory, particles are macroscopically slowed down by showing apparently elongated retention times inside the pores in both cases. However, detailed analysis of the particles' 3D trajectories shows that in viscous solvents, the particles are microscopically slowed down, showing decreased microscopic steps proportional to the increment of the viscosity. In contrast, the particles in sticky pores are microscopically active by showing limited reduction of the step sizes. The inconsistent diffusion behaviors observed at different length scales in sticky pores—macroscopically active but microscopically slow—are possibly caused by non-Brownian motion due to a heterogeneous environment and long-range attractive interaction rather than direct adsorption on the wall. This study shows that it is possible to differentiate slow diffusions in confined environments caused by different mechanisms using 3D SPT techniques.

The liquid–liquid interface is also frequently used in industrial processes such as partition and separation. Molecules diffuse to and at the interface, which is important to molecular partition. In nano- to mesoporous substrates, the curvature of the liquid–liquid interface can be quite large. However, despite the progress made in theoretical studies, how molecular diffusion is affected by a large curvature is largely unclear owing to experimental challenges. Zhong et al. (59) used expanded astigmatic PSF to study 3D trajectories of polystyrene nanoparticles diffusing on a highly curved water-silicone oil interface on oil droplets. They were able to recover particle trajectories on oil droplets with a size of ~400 nm to several micrometers (**Figure 7*a***). Unexpectedly, they found that the diffusion slows down significantly when the curvature becomes larger, or the oil droplet becomes smaller (**Figure 7*b***). A diffusion-induced droplet deformation and interface fluctuation model is proposed to explain the unexpected experimental results (**Figure 7*c***). This study suggests that molecular processes may be significantly different on highly curved interfaces such as those on lipid vesicles, micelles, emulsions, and droplets, or a chromatographic stationary phase attached to the wall of nanopores to mesopores. It would be interesting to further investigate molecular transport and chemical reactions on these highly curved interfaces.

## 4.4. Monitoring Particles in the 3D Space Under Micromanipulation

Controlled 3D positioning and delivery of particles in a contactless manner are important topics in modern analytical techniques. How to achieve this is still challenging, but the ability to monitor the particles in a confined to semi-open 3D space helps to design these micromanipulation systems. This can be achieved using 3D SPT techniques.

For example, Yu et al. (77) used a nanopipette to deliver polystyrene nanoparticles and capture them with an electrically charged substrate at designated locations. The delivery and positioning

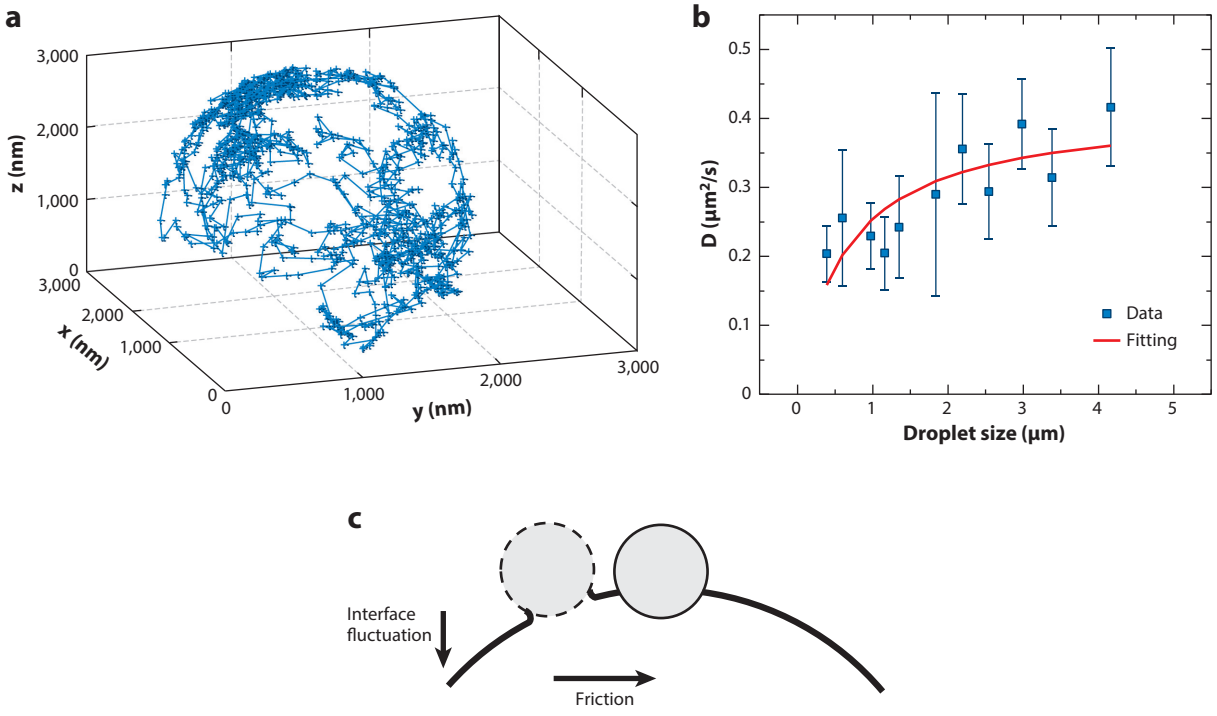


**Figure 7**

Particle diffusing on a water-oil droplet interface. (*a*) A representative 3D trajectory of a 100-nm nanoparticle diffusing on a 2,600-nm oil droplet surface. (*b*) Diffusion slows down as the droplet becomes smaller. (*c*) Proposed diffusion-induced droplet deformation and interface fluctuation model. Adapted with permission from Reference 59. Copyright 2017, American Chemical Society.

were achieved by balancing the pressure-driven flow in the pipette tip and the electric attractive force from the substrate. They used a double-helix PSF to monitor the whole controlled delivery process in real time with a precision of tens of nanometers. They observed that, as the nanoparticles approached the substrate, they experienced hindered diffusion and directed motion under the forces exerted on them. This study demonstrates that real-time monitoring and manipulation in the 3D space at the level of individual nanoparticles can be achieved, which is important to a variety of applications, such as surface patterning and drug delivery using colloidal nanoparticles.

Similarly, Sandoghdar and coworkers (69) used the i-SACT technique to show that a fluidic slit with appropriately tailored topography has a spatially modulated electrostatic potential that can trap and levitate charged particles in solution for up to several hours. They show that particles with different materials, such as gold, polymer, and lipid vesicles with varying diameters of tens of nanometers, can all be trapped without external intervention. The stability of the electrostatic trap can be easily tuned by changing the system shape, charge, and medium ionic strength. Because these kinds of traps can be easily combined with other micromanipulation techniques, it is expected that they can have a broad range of applications in contactless confining, sorting, or assembling of biomolecules to nanoobjects.

## 5. CONCLUSION AND FUTURE PERSPECTIVE

We have reviewed several frequently used 3D SPT techniques. Especially of interest are those based on PSF engineering, which are simple in instrumentation and inexpensive. They can be

easily adapted and used by many researchers, including analytical chemists. Corresponding data analysis methods for PSF engineering are briefly discussed with an emphasis on irregular PSF patterns. Thus far, there are a remarkably limited number of 3D SPT studies in the field of analytical chemistry. A few important case studies are presented with a focus on understanding mass transport in confined environments, which is important to many analytical techniques. The presented studies demonstrate the great potential of 3D SPT not only for these techniques but also far beyond, including solving problems in human health and renewable energy, such as heterogeneous catalysis and drug delivery. It can be envisioned that significant breakthroughs will be made in the near future in the quantitative understanding of nanoconfinement effects at the single-molecule and single-nanopore levels, which will have a profound impact on solving the aforementioned problems. In summary, these techniques are still in their infancy, and much work is needed in the future to improve these techniques and expand their applications. Three specific issues in need of further research are the following.

First, the most relevant issue to the topic of this review is the capability of 3D SPT to overcome challenges in observing molecular processes in a real medium, e.g., porous materials, which have strong scattering and background fluorescence from impurities. This problem can be alleviated using two approaches: (*a*) Improving the instrument. We noticed that efforts have already been made to combine other techniques, such as light sheet illumination, to reduce the background (106). We anticipate that these techniques will soon be applied to solve analytical chemical problems. (*b*) Developing new data analysis methods. More robust data analysis methods are needed, which can minimize the impact of high background and low signal problems in single-molecule imaging. In this sense, DNN is a highly potential method to achieve this goal.

Second, a practical challenge of current SPT techniques is the low throughput, i.e., only one or a few particles can be tracked in one experiment. The expanded image patterns in engineered PSFs make this problem worse. To increase the throughput, one can increase the particle density, which will cause two new problems: (*a*) the particle images overlap with each other, which harms 3D localization, and (*b*) the connection of dots between frames into 3D trajectories in the presence of a high density of particles becomes challenging. However, these problems can also be alleviated by neural networks–based artificial intelligence. DNNs show great resistance to interfering background (e.g., signal from an overlapping neighboring particle) in image pattern recognition, which makes simultaneous tracking of multiple particles possible. Additional work could be accomplished by introducing recurrent neural networks, which have superior performance in recognizing and predicting a time sequence, for dot connection between frames. With the help of deep learning methods, we expect that multiple particle tracking can be developed, which will significantly move this field forward.

Third, there is a need for the use of nonfluorescent probes. Nonfluorescent particles such as gold nanoparticles have become more popular in recent years because of their many advantages, such as high signal, nonbleaching nature, tunable shape, and tunable resonance wavelength. These particles need to be detected using other modes such as differential interference contrast microscopy, which has a unique, non-Airy disc pattern for point objects. They can be used in a broad range of fields and provide complementary information to that from fluorescent studies. How to develop 3D particle tracking technique using these nontraditional detection schemes remains to be investigated.

## DISCLOSURE STATEMENT

The authors are not aware of any affiliations, memberships, funding, or financial holdings that might be perceived as affecting the objectivity of this review.

## ACKNOWLEDGMENTS

The work is supported by the Department of Chemistry at North Carolina State University and the Department of Chemistry, Georgia State University.

## LITERATURE CITED

1. Rust MJ, Bates M, Zhuang X. 2006. Sub-diffraction-limit imaging by stochastic optical reconstruction microscopy (STORM). *Nat. Methods* 3:793–96
2. Saxton MJ, Jacobson K. 1997. Single-particle tracking: applications to membrane dynamics. *Annu. Rev. Biophys. Biomol. Struct.* 26:373–99
3. von Diezmann A, Shechtman Y, Moerner WE. 2017. Three-dimensional localization of single molecules for super resolution imaging and single-particle tracking. *Chem. Rev.* 117:7244–75
4. Stender AS, Marchuk K, Liu C, Sander S, Meyer MW, et al. 2013. Single cell optical imaging and spectroscopy. *Chem. Rev.* 113:2469–527
5. Sambur JB, Chen T-Y, Choudhary E, Chen G, Nissen EJ, et al. 2016. Sub-particle reaction and photocurrent mapping to optimize catalyst-modified photoanodes. *Nature* 530:77–80
6. Han R, Ha JW, Xiao CX, Pei YC, Qi ZY, et al. 2014. Geometry-assisted three-dimensional superlocalization imaging of single-molecule catalysis on modular multilayer nanocatalysts. *Angew. Chem. Int. Ed.* 53:12865–69
7. Chen KH, Boettiger AN, Moffitt JR, Wang S, Zhuang X. 2015. Spatially resolved, highly multiplexed RNA profiling in single cells. *Science* 348:aaa6090
8. Boettiger AN, Bintu B, Moffitt JR, Wang S, Beliveau BJ, et al. 2016. Super-resolution imaging reveals distinct chromatin folding for different epigenetic states. *Nature* 529:418–22
9. Wang C, Han B, Zhou R, Zhuang X. 2016. Real-time imaging of translation on single mRNA transcripts in live cells. *Cell* 165:990–1001
10. Zong C, Lu S, Chapman AR, Xie XS. 2012. Genome-wide detection of single-nucleotide and copy-number variations of a single human cell. *Science* 338:1622–26
11. Taniguchi Y, Choi PJ, Li G-W, Chen H, Babu M, et al. 2010. Quantifying *E. coli* proteome and transcriptome with single-molecule sensitivity in single cells. *Science* 329:533–38
12. Gebhardt JCM, Suter DM, Roy R, Zhao ZW, Chapman AR, et al. 2013. Single-molecule imaging of transcription factor binding to DNA in live mammalian cells. *Nat. Methods* 10:421–26
13. Kural C, Kim H, Syed S, Goshima G, Gelfand VI, Selvin PR. 2005. Kinesin and dynein move a peroxisome in vivo: A tug-of-war or coordinated movement? *Science* 308:1469–72
14. Kural C, Serpinskaya AS, Chou Y-H, Goldman RD, Gelfand VI, Selvin PR. 2007. Tracking melanosomes inside a cell to study molecular motors and their interaction. *PNAS* 104:5378–82
15. Kusumi A, Tsunoyama TA, Hirosawa KM, Kasai RS, Fujiwara TK. 2014. Tracking single molecules at work in living cells. *Nat. Chem. Biol.* 10:524–32
16. Shen H, Tauzin LJ, Baiyasi R, Wang WX, Moringo N, et al. 2017. Single particle tracking: from theory to biophysical applications. *Chem. Rev.* 117:7331–76
17. Axelrod D. 1981. Cell-substrate contacts illuminated by total internal reflection fluorescence. *J. Cell Biol.* 89:141–45
18. Bevan MA, Prieve DC. 2000. Hindered diffusion of colloidal particles very near to a wall: revisited. *J. Chem. Phys.* 113:1228–36
19. Eichmann SL, Anekal SG, Bevan MA. 2008. Electrostatically confined nanoparticle interactions and dynamics. *Langmuir* 24:714–21
20. Honciuc A, Harant AW, Schwartz DK. 2008. Single-molecule observations of surfactant diffusion at the solution-solid interface. *Langmuir* 24:6562–66
21. Skaug MJ, Mabry JN, Schwartz DK. 2014. Single-molecule tracking of polymer surface diffusion. *J. Am. Chem. Soc.* 136:1327–32
22. Walder R, Nelson N, Schwartz DK. 2011. Single molecule observations of desorption-mediated diffusion at the solid-liquid interface. *Phys. Rev. Lett.* 107:156102

23. Higgins DA, Park SC, Tran-Ba KH, Ito T. 2015. Single-molecule investigations of morphology and mass transport dynamics in nanostructured materials. *Annu. Rev. Anal. Chem.* 8:193–216
24. Higgins DA, Tran-Ba KH, Ito T. 2013. Following single molecules to a better understanding of self-assembled one-dimensional nanostructures. *J. Phys. Chem. Lett.* 4:3095–103
25. Han R, Wang GF, Qi SD, Ma CB, Yeung ES. 2012. Electrophoretic migration and axial diffusion of individual nanoparticles in cylindrical nanopores. *J. Phys. Chem. C* 116:18460–68
26. Ma CB, Han R, Qi SD, Yeung ES. 2012. Selective transport of single protein molecules inside gold nanotubes. *J. Chromatogr. A* 1238:11–14
27. Liao Y, Yang SK, Koh K, Matzger AJ, Biteen JS. 2012. Heterogeneous single-molecule diffusion in one-, two-, and three-dimensional microporous coordination polymers: directional, trapped, and immobile guests. *Nano Lett.* 12:3080–85
28. Kisley L, Chen JX, Mansur AP, Shuang B, Kourentzi K, et al. 2014. Unified superresolution experiments and stochastic theory provide mechanistic insight into protein ion-exchange adsorptive separations. *PNAS* 111:2075–80
29. Cooper JT, Peterson EM, Harris JM. 2013. Fluorescence imaging of single-molecule retention trajectories in reversed-phase chromatographic particles. *Anal. Chem.* 85:9363–70
30. Dong B, Pei YC, Zhao F, Goh TW, Qi ZY, et al. 2018. In situ quantitative single-molecule study of dynamic catalytic processes in nanoconfinement. *Nat. Catal.* 1:135–40
31. Speidel M, Jonáš A, Florin E-L. 2003. Three-dimensional tracking of fluorescent nanoparticles with subnanometer precision by use of off-focus imaging. *Opt. Lett.* 28:69–71
32. Gu Y, Di XW, Sun W, Wang GF, Fang N. 2012. Three-dimensional super-localization and tracking of single gold nanoparticles in cells. *Anal. Chem.* 84:4111–17
33. Toprak E, Balci H, Blehm BH, Selvin PR. 2007. Three-dimensional particle tracking via bifocal imaging. *Nano Lett.* 7:2043–45
34. Ram S, Prabhat P, Chao J, Ward ES, Ober RJ. 2008. High accuracy 3D quantum dot tracking with multifocal plane microscopy for the study of fast intracellular dynamics in live cells. *Biophys. J.* 95:6025–43
35. Juette MF, Bewersdorf J. 2010. Three-dimensional tracking of single fluorescent particles with submillisecond temporal resolution. *Nano Lett.* 10:4657–63
36. Prabhat P, Ram S, Ward ES, Ober RJ. 2004. Simultaneous imaging of different focal planes in fluorescence microscopy for the study of cellular dynamics in three dimensions. *IEEE Trans. NanoBiosci.* 3:237–42
37. Ram S, Prabhat P, Ward ES, Ober RJ. 2009. Improved single particle localization accuracy with dual objective multifocal plane microscopy. *Opt. Express* 17:6881–98
38. Wells NP, Lessard GA, Goodwin PM, Phipps ME, Cutler PJ, et al. 2010. Time-resolved three-dimensional molecular tracking in live cells. *Nano Lett.* 10:4732–37
39. Perillo EP, Liu Y-L, Huynh K, Liu C, Chou C-K, et al. 2015. Deep and high-resolution three-dimensional tracking of single particles using nonlinear and multiplexed illumination. *Nat. Commun.* 6:7874
40. Lessard GA, Goodwin PM, Werner JH. 2007. Three-dimensional tracking of individual quantum dots. *Appl. Phys. Lett.* 91:224106
41. Cang H, Wong CM, Xu CS, Rizvi AH, Yang H. 2006. Confocal three dimensional tracking of a single nanoparticle with concurrent spectroscopic readouts. *Appl. Phys. Lett.* 88:223901
42. Ragan T, Huang H, So P, Gratton E. 2006. 3D particle tracking on a two-photon microscope. *J. Fluoresc.* 16:325–36
43. Sriram I, Walder R, Schwartz DK. 2012. Stokes–Einstein and desorption-mediated diffusion of protein molecules at the oil–water interface. *Soft Matter* 8:6000–3
44. Du K, Liddle JA, Berglund AJ. 2012. Three-dimensional real-time tracking of nanoparticles at an oil–water interface. *Langmuir* 28:9181–88
45. Dinsmore AD, Weeks ER, Prasad V, Levitt AC, Weitz DA. 2001. Three-dimensional confocal microscopy of colloids. *Appl. Opt.* 40:4152–59

46. Jiang C, Kaul N, Campbell J, Meyhofer E. 2017. A novel dual-color bifocal imaging system for single-molecule studies. *Rev. Sci. Instrum.* 88:053705
47. Sun W, Marchuk K, Wang G, Fang N. 2010. Autocalibrated scanning-angle prism-type total internal reflection fluorescence microscopy for nanometer-precision axial position determination. *Anal. Chem.* 82:2441–47
48. Kihm K, Banerjee A, Choi C, Takagi T. 2004. Near-wall hindered Brownian diffusion of nanoparticles examined by three-dimensional ratiometric total internal reflection fluorescence microscopy (3-D R-TIRFM). *Exp. Fluids* 37:811–24
49. Chen T, Dong B, Chen KC, Zhao F, Cheng XD, et al. 2017. Optical super-resolution imaging of surface reactions. *Chem. Rev.* 117:7510–37
50. Berndt M, Lorenz M, Enderlein J, Diez S. 2010. Axial nanometer distances measured by fluorescence lifetime imaging microscopy. *Nano Lett.* 10:1497–500
51. Nitzsche B, Ruhnow F, Diez S. 2008. Quantum-dot-assisted characterization of microtubule rotations during cargo transport. *Nat. Nanotechnol.* 3:552–56
52. Huang B, Wang W, Bates M, Zhuang X. 2008. Three-dimensional super-resolution imaging by stochastic optical reconstruction microscopy. *Science* 319:810–13
53. Zhao L, Zhong Y, Wei Y, Ortiz N, Chen F, Wang G. 2016. Microscopic movement of slow-diffusing nanoparticles in cylindrical nanopores studied with three-dimensional tracking. *Anal. Chem.* 88:5122–30
54. Pavani SRP, Thompson MA, Biteen JS, Lord SJ, Liu N, et al. 2009. Three-dimensional, single-molecule fluorescence imaging beyond the diffraction limit by using a double-helix point spread function. *PNAS* 106:2995–99
55. Thompson MA, Lew MD, Badieirostami M, Moerner W. 2009. Localizing and tracking single nanoscale emitters in three dimensions with high spatiotemporal resolution using a double-helix point spread function. *Nano Lett.* 10:211–18
56. Yajima J, Mizutani K, Nishizaka T. 2008. A torque component present in mitotic kinesin Eg5 revealed by three-dimensional tracking. *Nat. Struct. Mol. Biol.* 15:1119–21
57. Kao HP, Verkman AS. 1994. Tracking of single fluorescent particles in 3 dimensions—use of cylindrical optics to encode particle position. *Biophys. J.* 67:1291–300
58. Zhong Y, Wang G. 2018. Three-dimensional heterogeneous structure formation on a supported lipid bilayer disclosed by single-particle tracking. *Langmuir* 34:11857–65
59. Zhong Y, Zhao L, Tyrlik PM, Wang G. 2017. Investigating diffusing on highly curved water–oil interface using three-dimensional single particle tracking. *J. Phys. Chem. C* 121:8023–32
60. Grover G, Quirin S, Fiedler C, Piestun R. 2011. Photon efficient double-helix PSF microscopy with application to 3D photo-activation localization imaging. *Biomed. Opt. Express* 2:3010–20
61. Shechtman Y, Gustavssonn AK, Petrov PN, Dultz E, Lee MY, et al. 2017. Observation of live chromatin dynamics in cells via 3D localization microscopy using Tetrapod point spread functions. *Biomed. Opt. Express* 8:5735–48
62. Lew MD, Lee SF, Badieirostami M, Moerner WE. 2011. Corkscrew point spread function for far-field three-dimensional nanoscale localization of pointlike objects. *Opt. Lett.* 36:202–4
63. Jia S, Vaughan JC, Zhuang XW. 2014. Isotropic three-dimensional super-resolution imaging with a self-bending point spread function. *Nat. Photon.* 8:302–6
64. Li H, Chen DN, Xu GX, Yu B, Niu HB. 2015. Three dimensional multi-molecule tracking in thick samples with extended depth-of-field. *Opt. Express* 23:787–94
65. Sun Y, McKenna JD, Murray JM, Ostap EM, Goldman YE. 2009. Parallax: high accuracy three-dimensional single molecule tracking using split images. *Nano Lett.* 9:2676–82
66. Backer AS, Backlund MP, von Diezmann AR, Sahl SJ, Moerner WE. 2014. A bisected pupil for studying single-molecule orientational dynamics and its application to three-dimensional super-resolution microscopy. *Appl. Phys. Lett.* 104:193701
67. Wang GF, Stender AS, Sun W, Fang N. 2010. Optical imaging of non-fluorescent nanoparticle probes in live cells. *Analyst* 135:215–21
68. Holsteen AL, Lin DM, Kauvar I, Wetzstein G, Brongersma ML. 2019. A light-field metasurface for high-resolution single-particle tracking. *Nano Lett.* 19:2267–71

69. Krishnan M, Mojarad N, Kukura P, Sandoghdar V. 2010. Geometry-induced electrostatic trapping of nanometric objects in a fluid. *Nature* 467:692–95
70. Lenc K, Vedaldi A. 2015. *Understanding image representations by measuring their equivariance and equivalence*. Presented at the IEEE Conference on Computer Vision and Pattern Recognition, June 7–12, Boston, MA. **https://ieeexplore.ieee.org/document/7298701**
71. Jia Y, Shelhamer E, Donahue J, Karayev S, Long J, et al. 2014. Caffe: convolutional architecture for fast feature embedding. *MM'14: Proceedings of the 22nd ACM International Conference on Multimedia*, pp. 675–78. New York: ACM. **https://dl.acm.org/doi/10.1145/2647868.2654889**
72. Aguet F, Van De Ville D, Unser M. 2005. A maximum-likelihood formalism for sub-resolution axial localization of fluorescent nanoparticles. *Opt. Express* 13:10503–22
73. Small A, Stahlheber S. 2014. Fluorophore localization algorithms for super-resolution microscopy. *Nat. Methods* 11:267–79
74. Zhou YZ, Handley M, Caries G, Harvey AR. 2019. Advances in 3D single particle localization microscopy. *APL Photon*. 4:060901
75. Cheezum MK, Walker WF, Guilford WH. 2001. Quantitative comparison of algorithms for tracking single fluorescent particles. *Biophys. J.* 81:2378–88
76. Abraham AV, Ram S, Chao J, Ward ES, Ober RJ. 2009. Quantitative study of single molecule location estimation techniques. *Opt. Express* 17:23352–73
77. Yu Y, Sundaresan V, Bandyopadhyay S, Zhang YL, Edwards MA, et al. 2017. Three-dimensional super-resolution imaging of single nanoparticles delivered by pipettes. *ACS Nano* 11:10529–38
78. Sheetz MP, Turney S, Qian H, Elson EL. 1989. Nanometre-level analysis demonstrates that lipid flow does not drive membrane glycoprotein movements. *Nature* 340:284–88
79. Mitchell T. 1997. *Machine Learning*. New York: McGraw Hill
80. Collins M, Schapire RE, Singer Y. 2002. Logistic regression, AdaBoost and Bregman distances. *Mach. Learn.* 48:253–85
81. Zhong YN, Li C, Zhou HY, Wang GF. 2018. Developing noise-resistant three-dimensional single particle tracking using deep neural networks. *Anal. Chem.* 90:10748–57
82. Krizhevsky A, Sutskever I, Hinton GE. 2012. Imagenet classification with deep convolutional neural networks. *NIPS'12: Proceedings of the 25th International Conference on Neural Information Processing Systems*, Vol. 1, pp. 1097–1105. New York: ACM. **https://dl.acm.org/doi/10.5555/2999134.2999257**
83. He K, Zhang X, Ren S, Sun J. 2015. *Delving deep into rectifiers: Surpassing human-level performance on imagenet classification*. Presented at IEEE International Conference on Computer Vision, Dec. 7–13, Santiago. **https://ieeexplore.ieee.org/document/7410480**
84. LeCun Y. 2012. Learning invariant feature hierarchies. In Computer Vision—ECCV 2012. Workshops and Demonstrations. ECCV 2012. Lecture Notes in Computer Science, Vol. 7583, ed. A Fusiello, V Murino, R Cucchiara, pp. 496–505. Berlin: Springer
85. Kasche V, Lindqvist L. 1964. Reactions between the triplet state of fluorescein and oxygen. *J. Phys. Chem.* 68:817–23
86. Jackson EA, Hillmyer MA. 2010. Nanoporous membranes derived from block copolymers: from drug delivery to water filtration. *ACS Nano* 4:3548–53
87. Lebold T, Jung C, Michaelis J, Braeuchle C. 2009. Nanostructured silica materials as drug-delivery systems for doxorubicin: single molecule and cellular studies. *Nano Lett*. 9:2877–83
88. Shao ZP, Haile SM. 2004. A high-performance cathode for the next generation of solid-oxide fuel cells. *Nature* 431:170–73
89. Stocker M. 2008. Biofuels and biomass-to-liquid fuels in the biorefinery: catalytic conversion of lignocellulosic biomass using porous materials. *Angew. Chem. Int. Ed.* 47:9200–11
90. Yang SY, Yang J-A, Kim E-S, Jeon G, Oh EJ, et al. 2010. Single-file diffusion of protein drugs through cylindrical nanochannels. *ACS Nano* 4:3817–22
91. Yuhas BD, Smeigh AL, Samuel APS, Shim Y, Bag S, et al. 2011. Biomimetic multifunctional porous chalcogels as solar fuel catalysts. *J. Am. Chem. Soc.* 133:7252–55
92. Zhang J, Yu J, Zhang Y, Li Q, Gong JR. 2011. Visible light photocatalytic $H_2$-production activity of CuS/ZnS porous nanosheets based on photoinduced interfacial charge transfer. *Nano Lett*. 11:4774–79

93. Han J, Craighead HG. 2000. Separation of long DNA molecules in a microfabricated entropic trap array. *Science* 288:1026–29
94. Striemer CC, Gaborski TR, McGrath JL, Fauchet PM. 2007. Charge- and size-based separation of macromolecules using ultrathin silicon membranes. *Nature* 445:749–53
95. Chen W, Wu ZQ, Xia XH, Xu JJ, Chen HY. 2010. Anomalous diffusion of electrically neutral molecules in charged nanochannels. *Angew. Chem. Int. Ed.* 49:7943–47
96. Zhang L, Feng Q, Wang JL, Sun JS, Shi XH, Jiang XY. 2015. Microfluidic synthesis of rigid nanovesicles for hydrophilic reagents delivery. *Angew. Chem. Int. Ed.* 54:3952–56
97. Nagumo R, Takaba H, Nakao SI. 2008. Accelerated computation of extremely 'slow' molecular diffusivity in nanopores. *Chem. Phys. Lett.* 458:281–84
98. Yamaguchi A, Mekawy MM, Chen Y, Suzuki S, Morita K, Teramae N. 2008. Diffusion of metal complexes inside of silica-surfactant nanochannels within a porous alumina membrane. *J. Phys. Chem. B* 112:2024–30
99. Kievsky YY, Carey B, Naik S, Mangan N, Ben-Avraham D, Sokolov I. 2008. Dynamics of molecular diffusion of rhodamine 6G in silica nanochannels. *J. Chem. Phys.* 128:151102
100. Pfenniger M, Calzaferri G. 2000. Intrazeolite diffusion kinetics of dye molecules in the nanochannels of zeolite L, monitored by energy transfer. *ChemPhysChem* 1:211–17
101. Bluhm EA, Bauer E, Chamberlin RM, Abney KD, Young JS, Jarvinen GD. 1999. Surface effects on cation transport across porous alumina membranes. *Langmuir* 15:8668–72
102. Jiang XQ, Mishra N, Turner JN, Spencer MG. 2008. Diffusivity of sub-1,000 Da molecules in 40 nm silicon-based alumina pores. *Microfluid. Nanofluid.* 5:695–701
103. Kennard R, DeSisto WJ, Mason MD. 2010. Molecular diffusivity measurement through an alumina membrane using time-resolved fluorescence imaging. *Appl. Phys. Lett.* 97:213701
104. Ma CB, Yeung ES. 2010. Single molecule imaging of protein molecules in nanopores. *Anal. Chem.* 82:478–82
105. Wang DP, Wu HC, Schwartz DK. 2017. Three-dimensional tracking of interfacial hopping diffusion. *Phys. Rev. Lett.* 119:268001
106. Gustavsson AK, Petrov PN, Moerner WE. 2018. Light sheet approaches for improved precision in 3D localization-based super-resolution imaging in mammalian cells. *Opt. Express* 26:13122–47